Kinetic barriers to SNAREpin assembly in the regulation of membrane docking/priming and fusion

Feng Li (李峰)[a], Neeraj Tiwari[a], James E. Rothman[a,1], and Frederic Pincet[a,b,c,d,e,1]

[a]Department of Cell Biology, School of Medicine, Yale University, New Haven, CT 06520; [b]Nanobiology Institute, School of Medicine, Yale University, New Haven, CT 06520; [c]Laboratoire de Physique Statistique, Ecole Normale Supérieure, Paris Sciences et Lettres Research University, 75005 Paris, France; [d]Laboratoire de Physique Statistique, Université Paris Diderot Sorbonne Paris Cité, 75005 Paris, France; and [e]Laboratoire de Physique Statistique, Sorbonne Universités, Université Pierre et Marie Curie, Univ Paris 06, CNRS, 75005 Paris, France

Edited by Wolfhard Almers, Oregon Health & Science University, Portland, OR, and approved July 27, 2016 (received for review March 12, 2016)

Neurotransmission is achieved by soluble NSF attachment protein receptor (SNARE)-driven fusion of readily releasable vesicles that are docked and primed at the presynaptic plasma membrane. After neurotransmission, the readily releasable pool of vesicles must be refilled in less than 100 ms for subsequent release. Here we show that the initial association of SNARE complexes, SNAREpins, is far too slow to support this rapid refilling owing to an inherently high activation energy barrier. Our data suggest that acceleration of this process, i.e., lowering of the barrier, is physiologically necessary and can be achieved by molecular factors. Furthermore, under zero force, a low second energy barrier transiently traps SNAREpins in a half-zippered state similar to the partial assembly that engages calcium-sensitive regulatory machinery. This result suggests that the barrier must be actively raised in vivo to generate a sufficient pause in the zippering process for the regulators to set in place. We show that the heights of the activation energy barriers can be selectively changed by molecular factors. Thus, it is possible to modify, both in vitro and in vivo, the lifespan of each metastable state. This controllability provides a simple model in which vesicle docking/priming, an intrinsically slow process, can be substantially accelerated. It also explains how the machinery that regulates vesicle fusion can be set in place while SNAREpins are trapped in a half-zippered state.

SNAREpin assembly | fusion regulation | RRP refilling | Tomosyn | fluorescence anisotropy

In synaptic transmission, neurotransmitter-containing vesicles are docked and primed at the presynaptic plasma membrane, forming a readily releasable pool (RRP). Priming is achieved through partial association of v-soluble NSF attachment protein receptors (v-SNAREs) from the vesicle with t-SNAREs from the plasma membrane at their N-terminal subdomains. The vesicles discharge their contents into the synaptic cleft upon stimulation by elevated intracellular Ca^{2+} influx (1). After the vesicles release their cargo, a new batch of vesicles docks to the presynaptic membrane and their v-SNAREs associate with t-SNAREs to be primed for the next round of fusion (2, 3). This process refills the RRP. At fast synapses, the rate of vesicle refilling is ∼100 ms (4–6). The assembly of the fusion-competent protein complex includes the N-terminal association of the t- and v-SNAREs, and thus this association must occur within such a timeframe (1, 7–10). In the conventional progressive zippering model, the N-terminal layers of the SNAREs have been presumed as the point where the assembly process is started and hence has been thought to be rapid (11). However, recent studies show the N-terminal assembly has to reach the middle layers (around layer −1) to achieve meaningful binding affinity; zippering of this subdomain is the rate-limiting step of membrane fusion and takes minutes (12). How can these two timescales, 100 ms and minutes, be reconciled? Here we precisely quantify the rate of assembly and show that the slow rate of N-terminal zippering is due to a high activation energy barrier that has to be overcome. Previous reports indicated that fusion can be accelerated in vitro by preincubating the t-SNARE with the C-terminal region of the v-SNARE (11, 13). We demonstrate that this acceleration is due to a structural change of t-SNARE that results in lowering of the activation energy barrier and faster N-terminal assembly. We find that this acceleration is a general feature that can be achieved by other protein factors.

After the N termini of the SNAREs have assembled, their C-terminal regions have to further zipper up and provide enough energy to the membranes to induce fusion. Functionally, these two assembly steps are distinct (12). However, it remains unclear whether they are kinetically separated, i.e., whether there is a pause in the assembly process between them. Some biophysical studies have tackled this issue (9, 14–17). Notably, when a single SNARE complex is disassembled with optical tweezers, extrapolation of the applied force to zero leads to a continuous downhill energy landscape that prevents any pause (15). Synaptic vesicle fusion is strictly regulated by neuronal proteins such as Complexin and Synaptotagmin. Evidence suggests that these regulators may act on the half-zippered SNARE (17–20). Therefore, a kinetic pause between the N- and C-terminal zipperings would be a key factor for organizing the regulation machinery. Here, we establish the existence of this kinetic pause between the two assembly steps under zero force.

Results

N-Terminal Assembly Is Thermodynamically Favorable, but Kinetically Unfavorable. To study the initial assembly of the v-SNARE (VAMP2) and t-SNARE (a complex of Syntaxin1A and SNAP25), we first measured the interactions between the N-terminal peptide of VAMP2 (Vn peptide, VAMP2 residues 1–57) and the entire

Significance

Neurotransmission requires fusion of the synaptic vesicles that are closely apposed to the presynaptic membrane. This apposition is achieved through the initial association of proteins known as soluble NSF attachment protein receptors (SNAREs). After a neurotransmission event, other vesicles must be rapidly prepared for the next round of fusion. Here we find the kinetics of the initial formation of SNARE complexes are too slow to spontaneously achieve this process because of a high activation energy barrier, but can be accelerated by molecular factors. In addition, we show that a second energy barrier transiently traps the SNARE complexes in a half-zippered state. This pause provides time for the regulatory machinery that accurately controls synchronized neurotransmission to be set in place.

Author contributions: F.L. and F.P. designed research; F.L. and N.T. performed research; F.L., J.E.R., and F.P. analyzed data; and F.L. and F.P. wrote the paper.

The authors declare no conflict of interest.

This article is a PNAS Direct Submission.

[1]To whom correspondence may be addressed. Email: pincet@lps.ens.fr or james.rothman@yale.edu.

This article contains supporting information online at www.pnas.org/lookup/suppl/doi:10.1073/pnas.1604000113/-/DCSupplemental.

cytosolic domain of t-SNARE (Syntaxin1A residues 1–265 and SNAP25 residues 1–206, Fig. 1*A*), using isothermal titration calorimetry (ITC). Surprisingly, when Vn was titrated into t-SNARE solution, the heat spikes had the same amplitude as in water–water titration, indicating that no binding signal was detected (Fig. 1*B*). This was unexpected because the binding between the t- and the v-SNARE is mainly due to exothermic hydrophobic interactions between heptad repeat motifs (21, 22).

We also separately titrated the C-terminal subdomain of v-SNARE (Vc peptide, VAMP2 residues 58–94) and the entire cytosolic domain (CDV, VAMP2 residues 1–94) into t-SNARE. The titration with Vc generated a large heat signal, which gave an affinity constant, K_D, of about 440 nM and ΔH of about −19.1 kcal·mol^{-1} (Fig. 1*C* and Table S1). The reaction between CDV and t-SNARE generated more heat, with ΔH about −40.1 kcal·mol^{-1} and K_D about 130 nM (Fig. 1*D*). Because the generated heat is additive, ΔH of Vn binding to t-SNARE equals ΔH of CDV binding minus that of Vc. Thus, the reaction of Vn binding with t-SNARE corresponds to $\Delta H \sim -21$ kcal·mol^{-1}, which seems to contradict the experiment in Fig. 1*B*, in which Vn peptide was titrated into t-SNARE and did not produce any heat signal.

This apparent contradiction may be due to kinetic effects. To test this hypothesis, we mutated Vn, Vc, and CDV to contain a single cysteine residue in their sequences and labeled them with a fluorescent dye. We then monitored fluorescence anisotropy during their binding with t-SNARE. We found that Vn or Vc alone could bind t-SNARE. However, the rate of Vn assembling was much slower (Fig. 1*E* and Fig. S1*A*). We evaluated the on rates and affinity constants of Vn, Vc, and CDV binding to t-SNARE (Fig. 1 *E* and *F*, Fig. S1, and Table S2). These results showed that Vn, Vc, and CDV were all able to bind t-SNARE with similar K_D (85 nM for Vn, 170 nM for Vc, and 110 nM for CDV; Fig. 1*F*). The striking difference is that Vn assembled with t-SNARE much slower than Vc and CDV. The on rates for Vc and CDV assembly were similar, 6,000–7,000 M^{-1}·s^{-1}; whereas Vn assembled with t-SNARE at an on rate of only about 500 M^{-1}·s^{-1}.

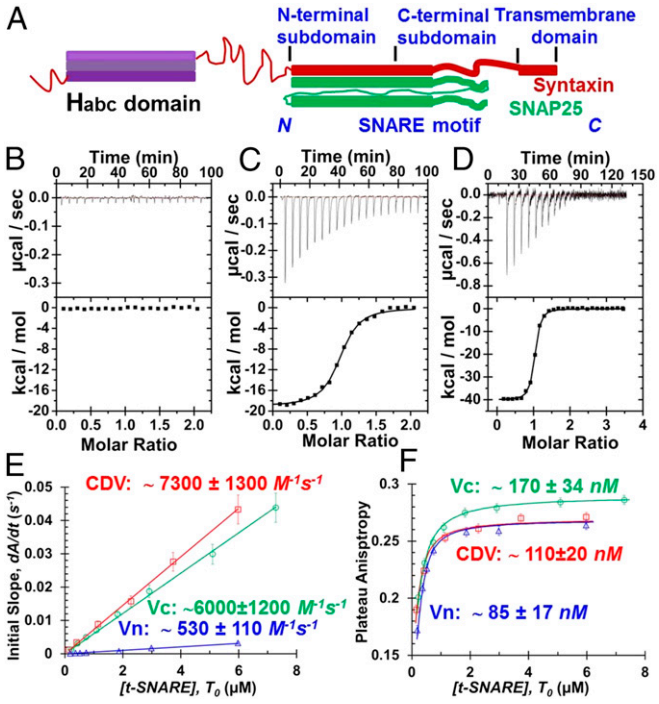

Fig. 1. Thermodynamics and kinetics of SNARE assembly. (*A*) Illustration of the structure of the t-SNARE. The SNARE motifs of Syntaxin1A (red) and SNAP25 (green) interact to form a complex. (*B–D*) ITC measurements of Vn peptide (*B*), Vc peptide (*C*), and CDV (*D*) assembling with the t-SNARE, respectively. Raw data in power vs. time during the injection are presented in *B–D*, *Upper*. Integrated heat vs. the molar ratio is plotted in *B–D*, *Lower*. The solid lines represented the best fits to the black squares. Thermodynamic parameters are listed in Table S1. (*E* and *F*) Fluorescence anisotropy experiments were performed to monitor the binding process of Vn (blue triangles), Vc (green circles), and CDV (red squares) to the t-SNARE at various concentrations at 26 °C, respectively. The anisotropy vs. time curves are presented in Fig. S1. (*E*) The initial binding rates were plotted vs. the concentration of t-SNARE (markers). The solid lines were fits to obtain the on rates. The error bars were determined from the SD of measurements in the anisotropy. (*F*) Plateau anisotropy values were plotted vs. the concentration of t-SNARE (markers). The solid lines were fits to obtain the affinity constants.

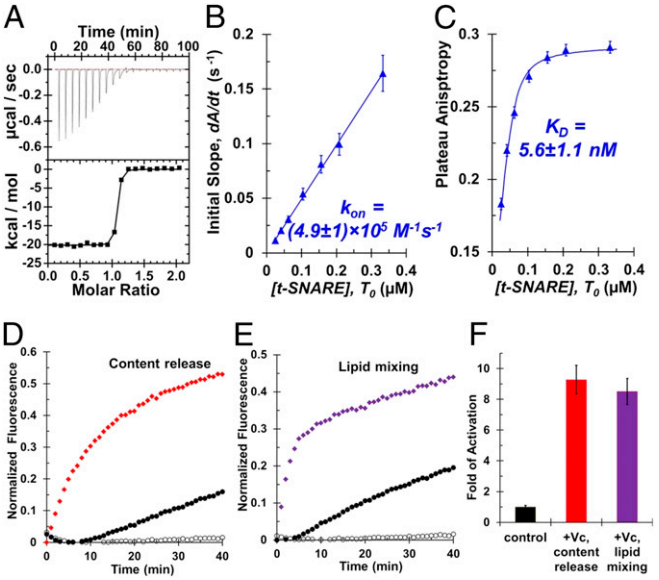

Fig. 2. Vc peptide activates N-terminal assembly both kinetically and thermodynamically. (*A*) ITC measurements of titration of Vn into prebound t-SNARE. To prebind the Vc peptide, the t-SNARE and Vc peptide (molar ratio 1:8) were incubated together at 37 °C for 60 min before titration. (*B* and *C*) Fluorescence anisotropy experiments were performed to monitor the binding process of Vn to prebound t-SNARE at various concentrations at 26 °C. The anisotropy vs. time curves are presented in Fig. S2*A*. Initial binding rates and plateau anisotropy values were plotted vs. concentration of t-SNARE, respectively, to obtain the on rate (*B*) and affinity constant (*C*). The error bars were determined from the SD of measurements in the anisotropy. (*D–F*) Vc peptide accelerates fusion rate in the content release assay. $CaCl_2$ was encapsulated inside full length t-SNARE–containing liposomes. When liposomes fused with nanodiscs containing full length v-SNARE, $CaCl_2$ was released from liposomes. Signals from both content release (*D*) and lipid mixing (*E*) were measured. When Vc prebound FLT (solid diamonds), both rates were accelerated. Positive control (solid black circles) represented fusion of t-liposomes and v-nanodiscs in the absence of prebinding. Negative control (open black circles) showed fusion between t-liposomes preincubated with cytosolic VAMP2 (CDV, residues 1–94) and v-nanodiscs. Approximately 10-fold activation due to prebinding of Vc was observed compared with positive control (*F*).

Reorganization of the N-Terminal Three-Helix Bundle of the t-SNARE Is Required to Accommodate the v-SNARE. To investigate the molecular basis of the kinetically unfavorable N-terminal assembly, we preincubated t-SNARE with Vc peptide. Vc prebound t-SNARE and formed a partial complex at their C termini, leaving the N terminus of t-SNARE available for Vn assembly. After the prebinding reached equilibrium, this t-SNARE/Vc mixture was titrated with Vn peptide (Fig. 2*A*). Large heat spikes due to Vn assembling with t-SNARE were measured, with ΔH about −20.2 kcal·mol^{-1}, which was consistent with the ΔH value calculated above, and K_D about 7 nM. The agreement in ΔH

suggests that the interactions between the binding residues on Vn and t-SNARE are not altered by Vc. Therefore, it seems that the prebinding of Vc to t-SNARE accelerated the N-terminal assembly of SNAREs.

We then used fluorescence anisotropy to measure the assembly kinetics of Vn binding to t-SNARE that was prebound with Vc (Fig. S2*A*). We determined the on rate and found that it was increased by ∼1,000 fold, to 4.9×10^5 $M^{-1}{\cdot}s^{-1}$ (Fig. 2*B*). Hence the previous kinetically unfavorable N-terminal assembly became highly favorable when t-SNARE was prebound with Vc. We also obtained the affinity constant from anisotropy measurements, $K_D \sim 5.6$ nM (Fig. 2*C*). Hence, the binding affinity of N-terminal assembly was improved from 85 nM to 5.6 nM upon Vc addition.

To test whether this prebinding-induced activation is limited to Vn peptide, we used the cytosolic domain of v-SNARE (CDV, VAMP2 residues 1–94) and similar results were obtained (*SI Text* and Fig. S3). The changes in the kinetic and thermodynamic parameters of CDV assembling with t-SNARE upon prebinding are close to those of Vn assembling. This suggests that, in both cases, activation originates from the same underlying molecular mechanism.

Previously, Melia et al. (11) reconstituted full-length t-SNARE and v-SNARE onto liposomes, respectively, and found that Vc peptide accelerated the rate of lipid mixing between t-SNARE liposomes and v-SNARE liposomes. Here we monitored both content mixing and lipid mixing, using nanodiscs and liposomes. The results showed that both lipid mixing and content release were accelerated (∼10-fold) through preincubating Vc peptide with t-SNARE liposomes (Fig. 2 *D*–*F*), consistent with previous reports (11, 13).

Fusion between v-SNARE nanodiscs and prebound t-SNARE liposomes is a result of the N- to C-directional zippering: Assembly is initialized on their N termini, followed by displacing the Vc peptide, and assembly continues on the C termini toward the transmembrane domains to induce bilayer merging. Because the N-terminal assembly of the SNAREs is intrinsically slow and can be significantly accelerated by Vc prebinding, the activation of liposome–nanodisc fusion by Vc is likely due to the acceleration of the N-terminal assembly.

Prebinding of t-SNARE with Vc is not physiologically meaningful as VAMP2 is not present in the plasma membrane before docking. However, other factors such as R-SNAREs [proteins containing a VAMP-like domain (VLD) with an arginine residue on the ionic layer] are in the plasma membrane and may play a similar role to that observed in vitro with Vc. Here, to check this general concept, we tested an R-SNARE, Tomosyn, which is found in the cytosol and the plasma membrane (23). Here we purified a C-terminal peptide of Tomosyn-1 (TSc, residues 1,076–1,115; Fig. S4*A*).

We first titrated TSc into the solution of the cytosolic domain of t-SNARE and found that TSc bound t-SNARE with a good affinity (K_D about 248 nM; Fig. S4*B*). Then we preincubated t-SNARE with TSc and titrated Vn into this mixture (Fig. 3*A*). The resulting thermograph showed that Vn assembled with prebound t-SNARE with a $K_D \sim 13.6$ nM and $\Delta H \sim -20.3$ kcal·mol^{-1}. In fluorescence anisotropy measurements, Vn assembled rapidly with t-SNARE that was prebound with TSc, with an on-rate k_{on} of about 5.1×10^5 $M^{-1}{\cdot}s^{-1}$ (Fig. 3*B*). In lipid-mixing fusion assays, when t-SNARE liposomes were preincubated with TSc, fusion with v-SNARE liposomes was accelerated about eightfold (Fig. 3*C*). These results show that, similarly to Vc, prebinding of TSc activates the t-SNARE and facilitates the N-terminal assembly. This finding suggests that such an activation effect is a general feature of the R-SNAREs.

These results show that (*i*) the N-terminal assembly of SNAREs is intrinsically slow, but can be significantly accelerated to satisfy synaptic vesicle docking/priming when t-SNARE is prebound with Vc or TSc; (*ii*) the N-terminal assembly is enthalpy driven and thermodynamically favorable; and (*iii*) N-terminal assembly is the limiting factor in fusion assays and acceleration of fusion is the direct result of activation on the N-terminal assembly.

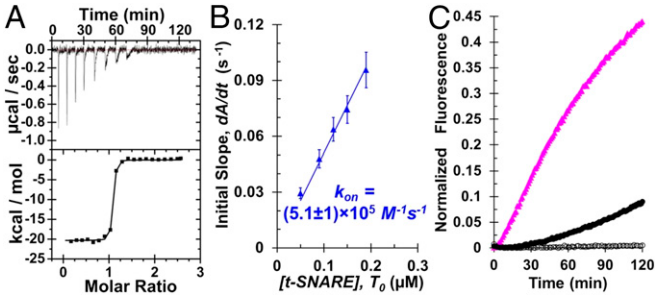

Fig. 3. Tomosyn-1 C peptide accelerates N-terminal assembly of the SNAREs. (*A*) TSc activates the t-SNARE in ITC measurements. Approximately 440 µM Vn peptide was titrated into ∼37 µM t-SNARE prebound with TSc. (*B*) Fluorescence anisotropy experiments were performed to monitor the binding process of Vn to t-SNARE prebound with TSc at various concentrations. Initial binding rates were plotted vs. the concentration of t-SNARE (solid triangles). The solid line is a fit to obtain the on rate. (*C*) TSc accelerates the fusion rate between t-liposomes and v-liposomes. Rates of lipid mixing were measured in the absence (black solid circles) and presence (pink triangles) of prebinding with TSc. Negative control (black open circles) showed fusion between t-liposomes preincubated with CDV and v-liposomes.

A previous study suggested that the function of Vc is to prevent a second Syntaxin binding to the t-SNARE that forms a 2:1 (Syntaxin:SNAP25 molar ratio) dead-end complex (13). Our experimental data have proved that the coexpressed t-SNARE, which was used in our study, contains Syntaxin and SNAP25 at a 1:1 molar ratio, and Vc accelerates the assembly of t- and v-SNARE even when SNAP25 is in large excess (*SI Text* and Fig. S5). Thus, the action of Vc goes beyond merely preventing dead-end complex formation, but induces a more profound change in t-SNARE. In the following we show that this change is related to a structural optimization of the t-SNARE.

The SNARE motif of the t-SNARE contains one helix from Syntaxin and two helices from SNAP25; it exhibits a three-helix-bundle structure on its N terminus and is unstructured on its C terminus (14, 24, 25). However, the structure of the postfusion SNARE complex exhibits a four-helix-bundle structure on both its N and C termini (Fig. 4*A*) (26). Therefore, during the N- to C-directional zippering process, t-SNAREs must restructure their three-helix bundles to accept the fourth helix from VAMP2 to form the four-helix bundle. Such helix reorganization costs energy. This is key to understanding the molecular basis of Vc accelerating the N-terminal assembly. In a previous study, we observed that when t-SNARE was prebound with a Vn peptide, X-ray crystallography showed a four-helix-bundle structure on its N terminus and such a four-helix configuration propagates to its C terminus, even though only three helices existed on the C terminus (12, 19). This is the helix continuation model. We hypothesize that, similarly, when Vc binds to t-SNARE, the C terminus of the SNARE complex is prestructured and adopts the four-helix-bundle conformation that is able to propagate and disrupt the initial three-helix bundle on the N terminus to form the same "four-helix-like" bundle structure as in the full-assembled SNARE (Fig. 4*A*). This prestructuring of the N-terminal region of the SNARE domain is validated by CD spectra, which show that t-SNARE has similar helical content when it is bound with either Vc or Vn peptide (Fig. 4*B*). Thus, a binding site is created on t-SNARE to facilitate the assembly with the N terminus of v-SNARE. Such a preformed binding site must occur before N-terminal assembly of the ternary complex to bypass the energy-costly reorganization of the t-SNARE and hence reduces the kinetic barrier (Fig. 4*C*).

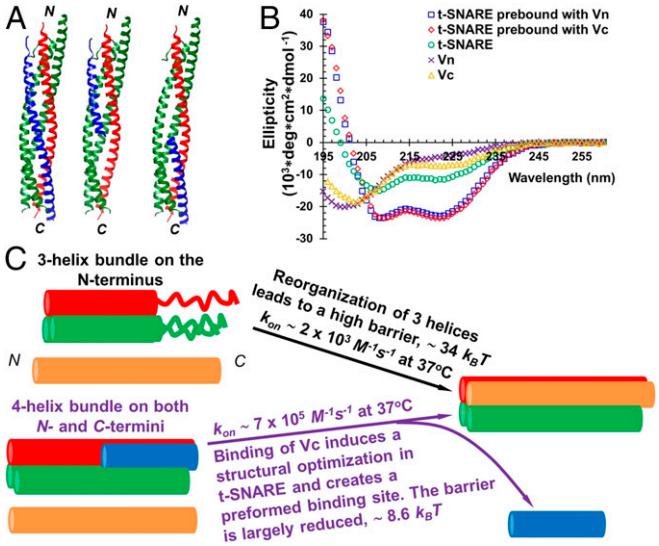

Fig. 4. Molecular basis for activation of the t-SNARE and acceleration of N-terminal assembly. (*A*) Helicity continuation model. When a Vn peptide binds the t-SNARE (*A*, *Center*) or a C-terminal peptide of R-SNARE prebinds the t-SNARE (*A*, *Right*), both N-terminal and C-terminal domains adopt the same four-helix bundle structure as in the postfusion, fully assembled SNARE complex (*A*, *Left*). (*B*) Vn and Vc peptides structure the t-SNARE to a similar extent. After incubating with Vn or Vc peptide, respectively, the CD spectra of SNAREs exhibited a similar amount of helical structure. The CD spectrum of t-SNARE was less structured, and CD spectra of Vn and Vc are largely unstructured. (*C*) Model of the molecular basis for activation of N-terminal assembly. In the N- to C-directional zippering, the N terminus of the t-SNARE needs to reorganize its three-helix bundle to accept the fourth helix from the v-SNARE. When a C-terminal peptide of R-SNARE prebinds the t-SNARE, the N terminus of v-SNARE is able to directly assemble with the preformed site and bypasses the helix reorganization.

Therefore, our data reveal that prebinding with the C-terminal peptide of an R-SNARE not only prestructures t-SNARE's C terminus, but also reorganizes its N-terminal three helices to create a preformed binding site for VAMP2. This reorganization provides the molecular basis for the facilitation of N-terminal assembly and may explain that Vc prevents non-fusogenic anti-parallel assembly (27).

Energy Landscape of SNAREpin Assembly Under Zero Force. Synaptic vesicle fusion is driven by the C-terminal assembly of the SNAREs, whereas vesicle docking and priming result from the N-terminal association. Thus, determining energy barriers during N- and C-terminal assembly is critical for understanding the kinetics of vesicle priming and fusion.

We performed fluorescence anisotropy measurements to monitor labeled Vn peptide assembling with t-SNARE or t-SNARE preincubated with Vc, at different temperatures T (Figs. S2 and S6). We then obtained the on-rate k_{on}, affinity constant K_D, and the off-rate k_{off} (through $K_D = k_{on}/k_{off}$), at each temperature (Table S2). Using the classical Arrhenius' equation, $k = Ae^{-(E_a/(k_BT))}$, where A is the preexponential factor, and k_B is the Boltzmann constant, we plotted k_{on} as a function of $1/T$ to obtain the activation barrier of the assembly reaction, $E_{a,on}$, both in the absence and in the presence of Vc prebinding (Fig. 5*A*). The striking finding here is that the activation barrier of the N-terminal assembly is extremely high, $E_{a,on} \sim 34\ k_BT$. This is the energy cost of prestructuring t-SNARE by opening the N-terminal three-helix bundle of t-SNARE to form a four-helix bundle with the N-terminal subdomain of v-SNARE. This high energy barrier is the reason why the N-terminal assembly is intrinsically slow and needs to be accelerated. In contrast, when t-SNARE is prebound with Vc, the energy barrier is substantially reduced to $E_{a,on} \sim 8.6\ k_BT$. As shown above, this large energy reduction is because such prebinding already opens the N-terminal three-helix bundle into a four-helix bundle-like configuration, and this explains why Vc accelerates N-terminal assembly.

Similarly, we plotted k_{off} as a function of $1/T$ to obtain the activation barrier of the disassociation, $E_{a,off}$ (Fig. 5*B*). As expected, the energy difference between the two states (Vn assembled state and unassembled state), $E_{a,off} - E_{a,on}$, is not altered

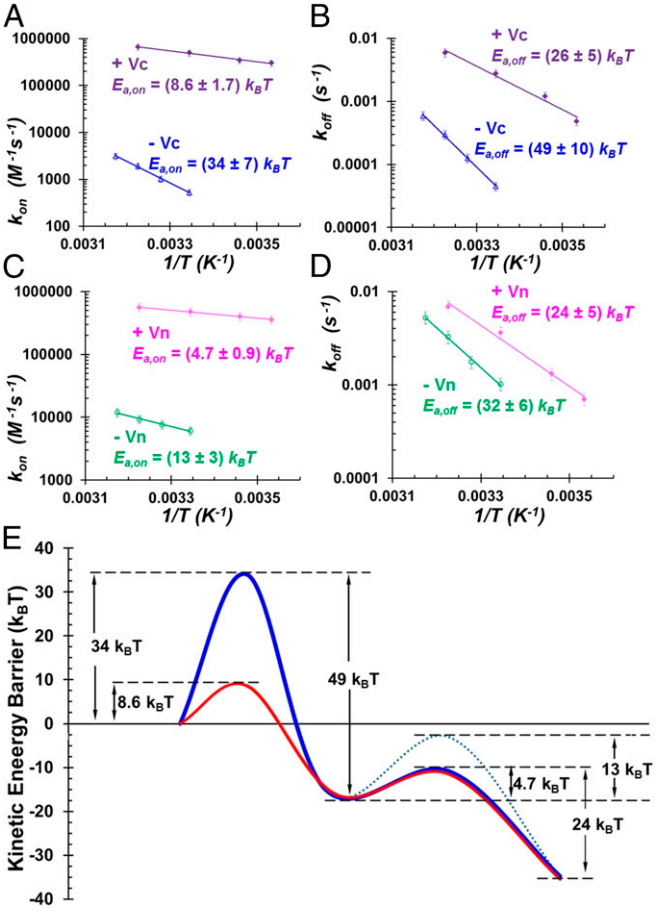

Fig. 5. Energy landscape of the kinetic barriers of the N- and C-terminal assemblies. (*A* and *B*) Fluorescence anisotropy experiments were performed to monitor the binding process of Vn to the t-SNARE at various concentrations and different temperatures in the absence (blue triangles) or presence (purple diamonds) of prebinding with excessive Vc, respectively. k_{on} and k_{off} were then plotted vs. $1/T$ to obtain the kinetic energy barriers of N-terminal association (*A*) and disassociation (*B*), respectively. (*C* and *D*) Fluorescence anisotropy experiments were performed to monitor the binding process of Vc to the t-SNARE in the absence (green circles) or presence (pink diamonds) of prebinding with excessive Vn, respectively. k_{on} and k_{off} were then plotted vs. $1/T$ obtain the kinetic energy barriers of C-terminal association (*C*) and disassociation (*D*), respectively. The error bars were determined from the SD of measurements in the anisotropy. (*E*) Energy landscape of the activation barriers. *E*, *Left* corresponds to the unbound states. The relative positions of the states (corresponding to the two minima in the plot) are free energies directly measured by ITC and florescence anisotropy. The activation energy barriers are determined by varying the temperature in the fluorescence anisotropy assay and may also be free energies (main text). In the absence of activation of the t-SNARE, the zippering pathway follows the blue solid curve. In the presence of activation, the zippering pathway follows the red solid curve. In both situations, the barrier of C-terminal assembly is low (~4.7 k_BT) as N-terminal zippering occurs first, which prestructures the C terminus of the t-SNARE. The dashed curve indicates the barrier of C-terminal assembly when N termini are not zippered.

by the prebinding: ~16 k_BT both in the presence and in the absence of the prebinding. Hence prebinding of Vc changes only the activation energy.

Via the same approach, we determined the energy barrier of the C-terminal assembly. We obtained $E_{a,\mathrm{on}} \sim 13\ k_BT$ for the C-terminal association. We also preincubated t-SNARE with a Vn peptide and measured the anisotropy of labeled Vc during its assembly with the prebound t-SNARE and obtained $E_{a,\mathrm{on}} \sim 4.7\ k_BT$ (Fig. 5 *C* and *D*). Similarly, the energy barrier of C-terminal assembly was also largely decreased when t-SNARE is prebound. Prebinding Vn changes the activation energies but not the energy difference, 18 k_BT, between the Vc unbound and Vc bound states.

For both energy barriers (N-terminal assembly and C-terminal assembly), the differences between the activation energies of the forward and backward reactions are very close to the free energy variations measured by ITC and fluorescence anisotropy. Even though this similarity is not a proof per se, it suggests that the energy barriers are not enthalpies but actual free energies.

With the activation barriers of both N- and C-terminal assemblies, we constructed an energy landscape to account for the N- to C-directional zippering (Fig. 5*E*). Due to topological constraints, C-terminal zippering occurs after N-terminal zippering, and hence the assembly substrate is the half-zippered SNARE intermediate. Therefore, the energy barrier of C-terminal assembly is reduced to 4.7 k_BT, which allows rapid zippering to satisfy submillisecond fast fusion. If t-SNARE is not activated for the N-terminal assembly, the energy landscape of the zippering pathway is described by the blue solid line in Fig. 5*E*. The energy barrier is high, 34 k_BT. When t-SNARE is activated upon prebinding with the C-terminal peptide of an R-SNARE, the energy landscape can be depicted by the red solid line in Fig. 5*E*. Here the barrier for N-terminal association is largely reduced to 8.6 k_BT, so that fast vesicle docking/priming becomes possible. There is an energy minimum between the two kinetic barriers, indicating the existence of the half-zippered SNARE intermediate (zippered on the N termini but not on the C termini).

Discussion

Zippering of the t- and v-SNAREs is required for membrane fusion. We have quantified the two main energy barriers that dictate the kinetics of this assembly. Our results provide critical insight into the understanding of two physiological processes: the refilling of the RRP and the organization of the regulatory machinery before fusion.

SNARE N-Terminal Assembly Must Be Accelerated for Rapid RRP Refilling. Due to topological constraints, the folding pathway of the SNAREs starts at their N termini. N-terminal assembly initializes their association and primes them by introducing a structural change in t-SNARE (12). As such, N-terminal assembly is part of the refilling process of the RRP. However, the assembly of these subdomains alone is the limiting step in SNARE zippering with an on rate of 1,900 $\mathrm{M^{-1}{\cdot}s^{-1}}$ at 37 °C. The density of SNAREs near the active zone of presynaptic membrane can be estimated to be of the order of ~100 μM, assuming that the gap between two synaptic vesicles before refilling the RRP is equal to their diameter (28, 29) and 70 copies of VAMP2 per vesicle (30). The resulting characteristic time is of the order of 10 s. This is too slow compared with the expected rate of refilling of the RRP (100 ms). Even though N-terminal assembly is energetically favorable, the three-helix bundle that composes the t-SNARE has to be opened and reorganized to accommodate the fourth helix coming from the v-SNARE. This process generates a high kinetic energy barrier, 34 k_BT. We propose three nonmutually exclusive scenarios to accelerate the assembly of the N-terminal domains as follows.

First, we have observed that when R-SNARE-like peptides are bound to t-SNARE, this reorganization of the three-helix bundle is already achieved before association with v-SNARE. The result is a faster assembly of the N-terminal subdomains with an on rate of $6.7 \times 10^5\ \mathrm{M^{-1}{\cdot}s^{-1}}$. Assuming 100 μM concentration, this would correspond to a characteristic time of 15 ms, consistent with a fast refilling of the RRP. Hence, we speculate that, in vivo, t-SNARE must also be prepared to accept the N-terminal subdomain of v-SNARE by opening up the groove where the fourth helix is inserted. Although full-length R-SNARE may occupy the entire SNARE motif of the t-SNARE and inhibit SNARE assembly, studies using the superior cervical ganglion neurons and the insulin-secreting cell line have revealed that Tomosyn enhances the formation of the SNARE complex, increases the fusion-competent readily releasable pool of synaptic vesicles, and enhances neurotransmitter release (31, 32). Yamamoto et al. (33) reported that the tail domain of Tomosyn binds the N-terminal half of Tomosyn's VLD and proposed that after PKA phosphorylation, the tail domain may be able to occupy the N-terminal half, so that only the C-terminal half of the VLD will be available to bind with the t-SNARE. Hence it is possible that this reorganization of t-SNARE may be achieved by an R-SNARE such as Tomosyn or, possibly, any other appropriate peptide in the vicinity of the plasma membrane, through interactions with other factors. Because these peptides are never present alone in vivo, such a mechanism requires that the N-terminal region of the VLD is blocked by another factor or template such as Tomosyn's tail domain or Munc18, leaving only the C-terminal region accessible.

Alternately, Munc18 is known to facilitate SNARE assembly (34, 35). X-ray crystallography showed that Vps33, the Sec1/Munc18 subunit in yeast, binds v-SNARE (36). It is probable that Munc18 binds VAMP2 and Syntaxin1A simultaneously, which would artificially increase their local concentrations. If this increase is beyond 100 mM, N-terminal assembly becomes fast enough to be with the timeframe of RRP refilling. Hence, Munc18 may act as a scaffold to facilitate the formation of the half-zippered SNARE.

The third scenario follows a recent suggestion that the t-SNARE is initially not assembled (37). It would assemble only upon binding with VAMP2. In this case, the kinetics may be different from what we observe here.

Pause in the Half-Zippered State Under Zero Force. In vivo and in vitro studies show that the machinery that regulates fusion seems to act on partial SNARE assembly (7–10, 17, 19, 38); for instance, studies on the cleavage of VAMP2 by tetanus toxin and Botulinum/B neurotoxin (7) and exocytosis measurements in adrenal chromaffin cells with overexpressed VAMP2 mutants (10) indicated the likelihood of partially folded intermediates. Surface force measurements indicated that partially zippered SNAREs were stable without any applied force (21, 39). Optical tweezers experiments observed an intermediate state when force of ~17 pN was applied. However, extrapolating the energy landscape to zero force, the intermediate state disappeared (15). We recently discovered distinct functional roles for N- and C-terminal zippering (12). These observations led to the conclusion that the regulatory machinery is set in place when the SNAREpin is kinetically trapped in the half-zippered state. Hence, it is surprising that this state vanishes under zero force. Here, we have unambiguously established this intermediate state exists with an energy barrier of ~5 k_BT (Fig. 5*E*), which corresponds to a lifetime of ~1 μs (40).

What is the origin of this contradiction? We propose that it can be due to an entropic effect. Indeed, in the optical tweezers experiments, the SNAREs are initially in the folded state and open up due to the stretching force field, and their entropy has been reduced close to the folded state. In contrast, in the present study, the SNAREs initially are in their relaxed, unperturbed state and possess their relaxation entropy. Modeling the unstructured SNAREs as polymers, we find that this entropy can

bring a few k_BT per SNARE that may be sufficient to account for the 5 k_BT activation energy we measured (*SI Text* and Fig. S7).

Assuming that the kinetic pause between N-terminal and C-terminal assemblies is around 1 μs would suggest that the intermediate state is very transient. Intermembrane repulsions due to the SNAREs themselves or other molecules will increase the duration of this state. However, negative regulators are needed to arrest the half-zippered state and clamp C-terminal assembly. Complexin has been reported to block progression of zippering (18, 19, 38). The k_{on} of Complexin binding to SNAREs is $\sim 3 \times 10^7$ $M^{-1} \cdot s^{-1}$ and its concentration is estimated in the 1- mM to 2-mM range (19, 41). Thus, if the intermembrane repulsion is large enough to prolong the lifetime of the intermediate state to ~20 μs, it is possible to recruit Complexin to half-zippered SNARE. Another possible scenario is that Complexin is recruited through binding with t-SNARE before association with v-SNARE, as we previously reported (17).

In vivo, sequential vesicle docking/priming and fusion are respectively governed by the assembly of the N- and C-terminal subdomains of SNAREs. The intrinsic high energy barrier with N-terminal assembly and subsequent low barrier in the C-terminal subdomain make it possible to enable or inhibit the docking/priming and fusion independently by using regulatory machineries to manipulate the assembly of SNAREs. Both phenomena are essential for precise spatial and temporal regulation of neurotransmission.

Materials and Methods

Below is a very brief description of the methods that were used. More details are given in *SI Materials and Methods*.

Protein Constructs, Expression, and Purification. Proteins were produced by expression in the BL-21 gold (DE3) *Escherichia coli* bacterial strain and purified as described before (12).

Lipid-Mixing Fusion Assay. Lipid mixing between full-length t-SNARE (FLT) liposomes and full-length VAMP2 (FLV) liposomes was measured by monitoring the dequenching of the DPPE-NBD fluorescence resulting from its dilution into the fused liposomes.

ITC Measurements. ITC experiments were performed with a Microcal ITC200 instrument similarly to what was described before (19).

Fluorescence Anisotropy. Fluorescence anisotropy was measured using T-format polarization. To obtain the kinetic parameters, we used the equations developed in a previous publication (12).

ACKNOWLEDGMENTS. We thank Dr. T. Melia for providing reagents and many helpful discussions. This work was supported by US National Institutes of Health Grant DK027044 (to J.E.R.) and French Agence Nationale de la Recherche Grant ANR-12-BSV5-0002 (to F.P.).

1. Jahn R, Fasshauer D (2012) Molecular machines governing exocytosis of synaptic vesicles. *Nature* 490(7419):201–207.
2. Südhof TC (1995) The synaptic vesicle cycle: A cascade of protein-protein interactions. *Nature* 375(6533):645–653.
3. Pyle JL, Kavalali ET, Piedras-Rentería ES, Tsien RW (2000) Rapid reuse of readily releasable pool vesicles at hippocampal synapses. *Neuron* 28(1):221–231.
4. Dittman JS, Regehr WG (1998) Calcium dependence and recovery kinetics of presynaptic depression at the climbing fiber to Purkinje cell synapse. *J Neurosci* 18(16):6147–6162.
5. Crowley JJ, Carter AG, Regehr WG (2007) Fast vesicle replenishment and rapid recovery from desensitization at a single synaptic release site. *J Neurosci* 27(20):5448–5460.
6. Moser T, Beutner D (2000) Kinetics of exocytosis and endocytosis at the cochlear inner hair cell afferent synapse of the mouse. *Proc Natl Acad Sci USA* 97(2):883–888.
7. Hua SY, Charlton MP (1999) Activity-dependent changes in partial VAMP complexes during neurotransmitter release. *Nat Neurosci* 2(12):1078–1083.
8. Xu T, et al. (1999) Inhibition of SNARE complex assembly differentially affects kinetic components of exocytosis. *Cell* 99(7):713–722.
9. Sørensen JB, et al. (2006) Sequential N- to C-terminal SNARE complex assembly drives priming and fusion of secretory vesicles. *EMBO J* 25(5):955–966.
10. Walter AM, Wiederhold K, Bruns D, Fasshauer D, Sørensen JB (2010) Synaptobrevin N-terminally bound to syntaxin-SNAP-25 defines the primed vesicle state in regulated exocytosis. *J Cell Biol* 188(3):401–413.
11. Melia TJ, et al. (2002) Regulation of membrane fusion by the membrane-proximal coil of the t-SNARE during zippering of SNAREpins. *J Cell Biol* 158(5):929–940.
12. Li F, et al. (2014) A half-zippered SNARE complex represents a functional intermediate in membrane fusion. *J Am Chem Soc* 136(9):3456–3464.
13. Pobbati AV, Stein A, Fasshauer D (2006) N- to C-terminal SNARE complex assembly promotes rapid membrane fusion. *Science* 313(5787):673–676.
14. Fiebig KM, Rice LM, Pollock E, Brunger AT (1999) Folding intermediates of SNARE complex assembly. *Nat Struct Biol* 6(2):117–123.
15. Gao Y, et al. (2012) Single reconstituted neuronal SNARE complexes zipper in three distinct stages. *Science* 337(6100):1340–1343.
16. Weber JP, Reim K, Sørensen JB (2010) Opposing functions of two sub-domains of the SNARE-complex in neurotransmission. *EMBO J* 29(15):2477–2490.
17. Li F, et al. (2011) Complexin activates and clamps SNAREpins by a common mechanism involving an intermediate energetic state. *Nat Struct Mol Biol* 18(8):941–946.
18. Giraudo CG, et al. (2009) Alternative zippering as an on-off switch for SNARE-mediated fusion. *Science* 323(5913):512–516.
19. Kümmel D, et al. (2011) Complexin cross-links prefusion SNAREs into a zigzag array. *Nat Struct Mol Biol* 18(8):927–933.
20. Wang J, et al. (2014) Calcium sensitive ring-like oligomers formed by synaptotagmin. *Proc Natl Acad Sci USA* 111(38):13966–13971.
21. Li F, et al. (2007) Energetics and dynamics of SNAREpin folding across lipid bilayers. *Nat Struct Mol Biol* 14(10):890–896.
22. Fasshauer D, Sutton RB, Brunger AT, Jahn R (1998) Conserved structural features of the synaptic fusion complex: SNARE proteins reclassified as Q- and R-SNAREs. *Proc Natl Acad Sci USA* 95(26):15781–15786.
23. Fujita Y, et al. (1998) Tomosyn: A syntaxin-1-binding protein that forms a novel complex in the neurotransmitter release process. *Neuron* 20(5):905–915.
24. Fasshauer D, Margittai M (2004) A transient N-terminal interaction of SNAP-25 and syntaxin nucleates SNARE assembly. *J Biol Chem* 279(9):7613–7621.
25. Munson M, Hughson FM (2002) Conformational regulation of SNARE assembly and disassembly in vivo. *J Biol Chem* 277(11):9375–9381.
26. Sutton RB, Fasshauer D, Jahn R, Brunger AT (1998) Crystal structure of a SNARE complex involved in synaptic exocytosis at 2.4 A resolution. *Nature* 395(6700):347–353.
27. Choi UB, Zhao M, Zhang Y, Lai Y, Brunger AT (2016) Complexin induces a conformational change at the membrane-proximal C-terminal end of the SNARE complex. *eLife* 5:e16886.
28. Fernández-Busnadiego R, et al. (2013) Cryo-electron tomography reveals a critical role of RIM1α in synaptic vesicle tethering. *J Cell Biol* 201(5):725–740.
29. Cole AA, Chen X, Reese TS (2016) A network of three types of filaments organizes synaptic vesicles for storage, mobilization, and docking. *J Neurosci* 36(11):3222–3230.
30. Takamori S, et al. (2006) Molecular anatomy of a trafficking organelle. *Cell* 127(4):831–846.
31. Baba T, Sakisaka T, Mochida S, Takai Y (2005) PKA-catalyzed phosphorylation of tomosyn and its implication in Ca2+-dependent exocytosis of neurotransmitter. *J Cell Biol* 170(7):1113–1125.
32. Cheviet S, et al. (2006) Tomosyn-1 is involved in a post-docking event required for pancreatic beta-cell exocytosis. *J Cell Sci* 119(Pt 14):2912–2920.
33. Yamamoto Y, et al. (2010) The tail domain of tomosyn controls membrane fusion through tomosyn displacement by VAMP2. *Biochem Biophys Res Commun* 399(1):24–30.
34. Shen J, Tareste DC, Paumet F, Rothman JE, Melia TJ (2007) Selective activation of cognate SNAREpins by Sec1/Munc18 proteins. *Cell* 128(1):183–195.
35. Voets T, et al. (2001) Munc18-1 promotes large dense-core vesicle docking. *Neuron* 31(4):581–591.
36. Baker RW, et al. (2015) A direct role for the Sec1/Munc18-family protein Vps33 as a template for SNARE assembly. *Science* 349(6252):1111–1114.
37. Ma C, Su L, Seven AB, Xu Y, Rizo J (2013) Reconstitution of the vital functions of Munc18 and Munc13 in neurotransmitter release. *Science* 339(6118):421–425.
38. Cho RW, et al. (2014) Genetic analysis of the Complexin trans-clamping model for cross-linking SNARE complexes in vivo. *Proc Natl Acad Sci USA* 111(28):10317–10322.
39. Wang YJ, et al. (2016) Snapshot of sequential SNARE assembling states between membranes shows that N-terminal transient assembly initializes fusion. *Proc Natl Acad Sci USA* 113(13):3533–3538.
40. Evans E (2001) Probing the relation between force–lifetime–and chemistry in single molecular bonds. *Annu Rev Biophys Biomol Struct* 30:105–128.
41. Pabst S, et al. (2002) Rapid and selective binding to the synaptic SNARE complex suggests a modulatory role of complexins in neuroexocytosis. *J Biol Chem* 277(10):7838–7848.
42. Wiederhold K, Fasshauer D (2009) Is assembly of the SNARE complex enough to fuel membrane fusion? *J Biol Chem* 284(19):13143–13152.

Supporting Information

Li et al. 10.1073/pnas.1604000113

SI Text

CDV Assembling with t-SNARE Is Accelerated by Prebinding of Vc. To test whether this prebinding-induced activation is limited to Vn peptide, we used the cytosolic domain of the v-SNARE (CDV, VAMP2 residues 1–94) to perform the experiments. In ITC measurement, we preincubated the t-SNARE with Vc peptide and then titrated CDV into this mixture (Fig. S3*A*). The thermodynamic parameters of this reaction were $K_D \sim 15$ nM and $\Delta H \sim -20.2$ kcal·mol^{-1} (Table S1), consistent with a previous report (42). It was notable that ΔH decreases from −40.1 kcal·mol^{-1} to −20.2 kcal·mol^{-1} upon prebinding of Vc. This reduction was expected. In the absence of Vc prebinding, CDV assembled with the t-SNARE on both N and C termini; whereas in the presence of Vc prebinding, assembly was initiated on the N-terminal subdomains of CDV and the t-SNARE, followed by displacement of Vc and further assembly of their C-terminal subdomains (13). Consequently, ΔH corresponding to C-terminal assembly canceled out. We also determined the on rate of CDV assembling with the t-SNARE prebound with Vc, using fluorescence anisotropy. In this measurement CDV contained a single cysteine residue on its N terminus at position 28 (S28C) and was labeled with Texas Red. As the assembly was initialized on the N termini of CDV and the t-SNARE and progressed to their C termini to displace Vc, we were able to directly measure the rate of N-terminal assembly and obtain $k_{on} \sim 5.1 \times 10^5$ M^{-1}·s^{-1} (Fig. S3*B*), similar to a previous report (10). This rate was similar to the on rate of Vn peptide binding with partially preassembled SNARE complex, suggesting that acceleration of N-terminal assembly through prebound t-SNARE is a general feature. The affinity constant obtained from anisotropy measurements was about $K_D \sim 1.2$ nM (Fig. S3*C*). Therefore, the prebinding of Vc to the t-SNARE facilitates CDV assembly both kinetically and thermodynamically. The changes in the kinetic and thermodynamic parameters of CDV assembling with t-SNARE upon prebinding are close to those of Vn assembling. This result suggests that, in both cases, activation originates from the same underlying molecular mechanism.

Coexpressed t-SNARE Contains Syntaxin and SNAP25 at 1:1 Molar Ratio. What is the molecular mechanism underlying the activation function of Vc peptide? A previous study suggested that the function of Vc is to prevent a second Syntaxin binding to the t-SNARE and forming the 2:1 (Syntaxin:SNAP25 molar ratio) dead-end complex (13). In our experiments, we always used coexpressed t-SNARE, which has a His-tag on the N terminus of SNAP25, whereas Syntaxin is tagless. It is likely that Syntaxin and SNAP25 prefold into a 1:1 complex in vivo when they are coexpressed in the cells. Moreover, during the purification, we used a Nickel-NTA affinity column to bind the His-tag on SNAP25. Hence a 2:1 (Syntaxin:SNAP25) complex is unlikely because excessive Syntaxin will be washed away. To test the actual molar ratio of coexpressed t-SNARE, we first used quantitative gel analysis. We expressed and purified Syntaxin and SNAP25 separately and determined their concentrations, respectively. We then mixed these separately expressed Syntaxin and SNAP25 at a 1:1 molar ratio and loaded the mixture to the same gel together with coexpressed t-SNARE (Fig. S5*A*). We used ImageJ to quantify the intensity of each protein band and determined the intensity ratio between Syntaxin and SNAP25 bands. The intensity ratio between Syntaxin and SNAP in coexpressed t-SNARE was 1.34 ± 0.05. When separately expressed Syntaxin and SNAP25 were mixed at a 1:1 molar ratio, the intensity ratio was 1.32 ± 0.04. The similarity between the intensity ratios suggests that coexpressed t-SNARE contains Syntaxin and SNAP25 at a 1:1 molar ratio.

Second, we reconstituted coexpressed t-SNARE into liposomes and preincubated them with an excess of SNAP25 at various concentrations, respectively, and measured their fusion rates with v-SNARE liposomes (Fig. S5*B*). Compared with a positive control (fusion of t-SNARE liposomes and v-SNARE liposomes in the absence added soluble SNAP25), the fusion rate became slower as the concentration of SNAP25 in excess was increased. Notably, the Syntaxin concentration in the fusion assay was measured to be ∼1.7 μM, and the highest concentration of added SNAP25 was 15.3 μM, which led to a molar ratio of 1:10 (Syntaxin:SNAP25). Moreover, when Vc was added into every preincubation with SNAP25 at various concentrations, the fusion rate was rescued and highly accelerated.

We also preincubated t-SNARE liposomes with an excess of soluble Syntaxin (the cytosolic domain of Syntaxin 1A residues 1–265) at various concentrations, respectively, and measured their fusion rates with v-SNARE liposomes (Fig. S5*C*). Similarly, fusion rates became slower when the concentration of added Syntaxin was increased.

Third, we mixed separately expressed soluble Syntaxin and SNAP25 at 1:1 and 1:10 molar ratios, respectively, and used fluorescence anisotropy to measure the kinetics of cytosolic VAMP2 (CDV) binding to these two mixtures (Fig. S5 *D* and *E*). The on rate of CDV binding to the 1:1 mixture was ∼(7.7 ± 1.6) × 10^3 M^{-1}·s^{-1}, similar to the rate for coexpressed t-SNARE. For the mixture with 1:10 molar ratio, the on rate was reduced to ∼(1.8 ± 0.3) × 10^3 M^{-1}·s^{-1} (Fig. S5*G*), which is consistent with the liposome–liposome fusion result that an excess of SNAP25 inhibits fusion rate. When Vc was added into the 1:10 mixture, with Syntaxin:SNAP25:Vc at a 1:10:8 molar ratio (Fig. S5*F*), the on rate was significantly accelerated to (4.8 ± 1.0) × 10^5 M^{-1}·s^{-1} (Fig. S5*G*).

Putting these results together, we are able to conclude the following: (*i*) The assembly between the t- and v-SNAREs is inhibited by an excess of either SNAP25 or Syntaxin. The reason for the SNAP25 inhibition of fusion is possibly the formation of a 1:2 (Syntaxin:SNAP25) dead-end complex, similar to the 2:1 (Syntaxin:SNAP25) dead-end complex that was proposed in previous reports. (*ii*) Our coexpressed t-SNARE contains Syntaxin and SNAP at a 1:1 molar ratio, as it is vulnerable to adding either extra Syntaxin or extra SNAP25, which induces the formation of a mismatched dead-end complex. (*iii*) Whether at 1:1 (Syntaxin:SNAP25) or 1:10 molar ratio, the assembly and fusion rates induced by the t- and v-SNAREs are intrinsically slow and need to be activated. (*iv*) Whether at 1:1 (Syntaxin:SNAP25) or 1:10 molar ratio, Vc is able to significantly accelerate the assembly and fusion rates between the t- and v-SNAREs. These results show that preventing the formation of a 2:1 dead-end complex is not sufficient to activate the t-SNARE or accelerate the assembly. Therefore, the molecular mechanism of Vc activation is most likely due to a structural optimization in the t-SNARE, as we proposed in the main text.

In the paper of Pobbati et al. (13), the authors suggest that they initially have an excess of Syntaxin leading to the formation of 2:1 dead-end complexes that are disrupted by addition of SNAP25. In our case, we used coexpressed t-SNARE, which is at a 1:1 molar ratio. It is difficult to compare our results with that of Pobbati et al. (13), because our starting materials (t-SNAREs) are purified differently. We also note that, in another paper (10), the same group reported an on rate, 2.35×10^5 M^{-1}·s^{-1}, for CDV binding to premixed Syntaxin, SNAP25, and Vc (residues 49–96), which was called the ΔN complex in their paper. This value is similar to the one we obtained.

Entropic Effect of the SNARE Assembly Under Force. What is the origin of the apparent contradiction between the single-molecule

experiments (no intermediate state at zero force) and our present results? We propose that it can be due to an entropic effect. Indeed, under a force f, the on rate can be written as $k_{on} = k_0.\exp(-\Delta E_{app}/k_BT) = k_0.\exp((-\Delta E - f\delta x)/k_BT)$, where k_0 is the attempt of escape frequency, ΔE_{app} is the apparent energy barrier under force, ΔE is the extrapolated energy barrier without force, and δx is the displacement along the force during zippering. When $f\delta x$ is larger than ΔE_{app}, the energy barrier vanishes under zero force. This is what was experimentally observed. However, in the single-molecule experiments, the SNAREs are initially in the folded state and open up due to the stretching force field (Fig. S7). The energy is measured at the disassembly/refolding transition. The proteins are already stretched before refolding because of the applied force. Hence, their entropy has been reduced close to the folded state. In contrast, in the present study, the SNAREs are initially in their relaxed, unperturbed state and possess their relaxation entropy. For an ideal polymer, the variation of entropy under a force f is $\Delta S = f\cdot((R(0)^2 - R(f)^2))/(T\cdot R(f))$, where $R(0)$ is the unperturbed end-to-end distance, $R(f)$ is the end-to-end distance under force f, and T is the temperature. This entropy can thus bring a free energy $T\Delta S = f\cdot((R(0)^2 - R(f)^2))/R(f)$. The typical force in optical tweezers at which transitions occur is ~10 pN. The radius $R(f)$ is ~12 nm, and $R(0)$ can be neglected (because of the square in the expression). With these values, the free energy gain is 120 pN·nm ~30 k_BT. This is an overestimate (SNAREs are not random polymers), but shows that the entropy change can bring a few k_BT per SNARE that may be sufficient to account for the 5-k_BT activation energy we measured.

SI Materials and Methods

Chemicals. The lipids used in this study, 1-palmitoyl-2-oleoyl-sn-glycero-3-phosphocholine (POPC), 1,2-dioleoyl-sn-glycero-3-(phospho-L-serine) (sodium salt) (DOPS), 1,2-dipalmitoyl-sn-glycero-3-phosphoethanolamine-*N*-(lissamine rhodamine B sulfonyl) (ammonium salt) (DPPE-Rho), and 1,2-dipalmitoyl-sn-glycero-3-phosphoethanolamine-*N*-(7-nitro-2–1,3-benzoxadiazol-4-yl) (ammonium salt) (DPPE-NBD), were purchased from Avanti Polar Lipids. Texas Red C2 Maleimide was purchased from Invitrogen. The 4-(2-hydroxyethyl)piperazine-1-ethanesulfonic acid (Hepes), potassium hydroxide (KOH), potassium chloride (KCl), glycerol, 2-mercaptoethanol, and Tris(2-carboxyethyl)phosphine hydrochloride (TCEP) were purchased from Sigma-Aldrich. All aqueous solutions were prepared using 18.2 M ultrapure water (purified with the Millipore MilliQ system).

Protein Constructs, Expression, and Purification.

Full-length t-SNARE complex (FLT). The full length t-SNARE complex, which includes full-length, wild-type mouse His6-SNAP25 and rat Syn1A, was produced by expression of the polycistronic plasmid pTW34 in the BL-21 gold (DE3) *E. coli* bacterial strain and purified as described before (11, 12).

Full-length VAMP2 (FLV). The full length VAMP2, which includes full-length, wild-type mouse VAMP2, was produced by expression of the plasmid pTW2 in the BL-21 gold (DE3) *E. coli* bacterial strain and purified as described before (11, 12).

Cytosolic t-SNARE complex. The soluble t-SNARE complex, made of the cytoplasmic domain of rat Syntaxin1A (residues 1–265) and mouse His6-SNAP25 (residues 1–206), was produced by coexpression of pJM57 and pJM72 plasmids in the BL-21 gold (DE3) *E. coli* bacterial strain and purified as described before (17, 21).

Cytosolic VAMP2 (CDV). The plasmid for CDV was produced by cloning VAMP2 into a pET SUMO vector containing N-terminal His_6 tag. The construct contains VAMP2 residues 1–94. This protein was produced by expression in the BL-21 gold (DE3) *E. coli* bacterial strain and purified as previously described (17, 21).

Cytosolic VAMP2 (CDV-S28C). The plasmid for CDV-S28C was produced by cloning into a pET SUMO vector containing an N-terminal His_6 tag. The construct contains VAMP2 residues 1–94 with a single point mutation S28C. This protein was produced by expression in the BL-21 gold (DE3) *E. coli* bacterial strain and purified as previously described (17, 21).

N-terminal subdomain of VAMP2 (Vn). The plasmid for the Vn was produced by cloning the N terminus of VAMP2 into a pCDFDuet-1 vector containing GST-PreScission-Vn (containing mouse VAMP2 N-terminal residues). The Vn constructs generated were Vn (VAMP2 residues 28–57) and Vn-S28C (VAMP2 residues 1–57, with a single cysteine mutation at position 28). These proteins were produced by expression in the BL-21 gold (DE3) *E. coli* bacterial strain and purified as previously described (12).

C-terminal subdomain of VAMP2 (Vc). The plasmid for Vc was produced by cloning the C terminus of VAMP2 into a pET SUMO vector containing N-terminal His_6 tag. The construct contains VAMP2 residues 58–94 with a single cysteine residue in the end of the sequence. This protein was produced by expression in the BL-21 gold (DE3) *E. coli* bacterial strain and purified as previously described (12).

Membrane scaffold protein. Membrane scaffold protein (MSP) was expressed by plasmid MSP1E3D1-pet28 (Addgene). Its expression and purification were previously described (12). After eluting MSP from the Nickel-NTA beads, its 6× His-tag was cleaved through overnight incubation at 4 °C with TEV protease.

SNARE–Liposome Reconstitution. The full-length t-SNARE complex was reconstituted with the acceptor lipid mix made of 85 mol% POPC and 15 mol% DOPS. Full-length VAMP2 was reconstituted with the donor lipid mix composed of 82 mol% POPC, 15 mol% DOPS, 1.5 mol% DPPE-RHO, and 1.5 mol% DPPE-NBD.

The SNARE liposomes were prepared using the standard detergent removal method, which was previously reported (11, 12). Typically, FLT liposomes had 400:1 lipid:protein ratio and the FLV liposomes had 200:1 lipid:protein ratio.

Preparation of FLT Liposomes with $CaCl_2$ Encapsulation. FLT liposomes with $CaCl_2$ encapsulation were prepared as described before (12). Briefly, 1,200 nmol DOPC was dried by nitrogen flow, followed by vacuum drying, and then resuspended with FLT in 400 μL buffer that contained 25 mM Hepes, 350 mM KCl, 1 mM DTT, 50 mM $CaCl_2$, and 1% OG. The mixture was vortexed vigorously for 30 min at room temperature. OG concentration was rapidly diluted by adding 1,000 μL buffer that contained 25 mM Hepes, 1 mM DTT, and 50 mM $CaCl_2$. The mixture was loaded into a Slide-A-Lyzer Dialysis Cassette (7K MWCO; Thermo Scientific) and dialyzed against 4 L buffer that contained 25 mM Hepes, 1 mM DTT, 175 mM KCl, and 4 g Bio-Beads SM-2 Adsorbents (Bio-Rad) overnight at 4 °C. Then the liposomes were collected from the dialysis cassette, mixed with 80% (wt/vol) Nycodenz at equal volume, and loaded into a centrifuge tube (Beckman). A total of 500 μL 30% (wt/vol) Nycodenz was laid over the sample, followed by 500 μL 20% (wt/vol) Nycodenz and 250 μL dialysis buffer, respectively, and then centrifuged for 4 h at 50,000 rpm (400,000 × *g*) at 4 °C. The final sample was collected at the interface between dialysis buffer and 20% Nycodenz.

To test whether the liposomes leak, 50 μL FLT liposomes and 2 μL 100 μM Mag-fluo-4 were loaded into the same well of a 96-well plate and gently mixed. A plate reader (Bio-Tek) was used to monitor the fluorescence of Mag-fluo-4 for 1 h at 37 °C. If there was no leakage problem, the fluorescence signal would remain stable without apparent increase. Then 10 μL of dodecyl maltoside was added to break up all of the liposomes; a sudden, significant increase of the fluorescence signal would be observed if $CaCl_2$ was indeed encapsulated inside the liposomes.

SNARE–Nanodiscs Preparation. Reconstitution of FLV on nanodiscs was performed following a protocol from a published work (12). Briefly, 300 nmol of 85 mol% POPC and 15 mol% DOPS were dried by nitrogen flow, followed by vacuum drying, and then

resuspended with MSP, FLV (tag cleaved), and a buffer that contained 25 mM Hepes, 400 mM KCl, 1 mM DTT, and OG. Final volume of the mixture was 300 μL and final OG concentration was 1%. The molar ratio of FLV:MSP:lipid was 4:1:60. The mixture was vortexed at room temperature for 30 min, followed by 3 h shaking at 4 °C. A total of 300 mg Bio-Beads SM-2 Adsorbents were added into the mixture, and then it was shaken overnight. In the next day, the solution mixture was separated from the adsorbents and purified by gel filtration, using the Superdex 200 column (GE Healthcare) and a running buffer containing 25 mM Hepes, 1 mM DTT, and 140 mM KCl. The SNARE–nanodisc sample was collected and concentrated to 100 μL by a centrifugal filter unit (Amicon).

Lipid-Mixing Fusion Assay. For a typical liposome–liposome fusion assay, 45 μL FLT liposomes was mixed with 15 μL buffer or peptide solution (final concentrations of lipids and peptide were ∼2 mM and ∼20 μM, respectively), incubated at 37 °C for 30 min, and then transferred to a 96-well FluoroNunc plates (Nalge Nunc) and kept at 37 °C for 5 min. The fusion reaction was initiated by adding 5 μL of FLV liposomes. Fusion between FLT liposomes and FLV liposomes was measured by monitoring the dequenching of the DPPE-NBD fluorescence resulting from its dilution into the fused liposomes, at 1-min intervals for 120 min, with excitation wavelength at 460 nm and emission wavelength at 538 nm, by a plate reader (Synergy H1 Hybrid Microplate Reader; Bio-Tek). After 120 min, 10 μL of 2.5% (wt/vol) n-dodecylmaltoside (Boehringer) was added to completely dissolve the liposomes. Measurement of the DPPE-NBD fluorescence was continued for another 40 min to obtain the DPPE-NBD fluorescence at infinite dilution. As reported previously (12), the normalized fluorescence was obtained by using the fluorescence intensity of DPPE-NBD during fusion divided by the average intensity of the DPPE-NBD fluorescence at infinite dilution.

Liposome–Nanodisc Content Mixing and Lipid-Mixing Assay. The liposome–nanodisc fusion assay was similar to the liposome–liposome lipid mixing assay and was described before (12). Typically, 50 μL of FLT liposome with $CaCl_2$ encapsulation was mixed with 15 μL buffer or Vc peptide, incubated at 37 °C for 30 min, and then transferred to 96-well FluoroNunc plates. A total of 1.1 μL Mag-fluo-4 at 100 μM was added for the content mixing assay. The mixture was kept at 37 °C for 5 min. The fusion reaction was initiated by adding 2.5 μL of FLV nanodiscs. Both lipid mixing and content mixing were measured in parallel. For the lipid-mixing assay, the nanodisc contained 82 mol% POPC, 15 mol% DOPS, 1.5 mol% DPPE-RHO, and 1.5 mol% DPPE-NBD, and Mag-fluo-4 was not added into the bulk buffer. Lipid mixing was measured by monitoring the dequenching of the DPPE-NBD fluorescence resulting from its dilution into the fused liposomes, with excitation wavelength at 460 nm and emission wavelength at 538 nm. For the content-mixing assay, the nanodisc contained 85 mol% POPC, 15 mol% DOPS, and no fluorescent lipid, and 1.1 μL Mag-fluo-4 was added into the bulk buffer. Content mixing was measured by monitoring the increase of the fluorescence of Mag-fluo-4 resulting from its binding to Ca^{2+} as $CaCl_2$ was released from the FLT liposomes to the bulk buffer during fusion pore opening, with excitation wavelength at 480 nm and emission wavelength at 520 nm. After 60 min, 10 μL of 2.5% (wt/vol) n-dodecylmaltoside was added to completely dissolve all of the liposomes. Measurement of the Mag-fluo-4 (and DPPE-NBD) fluorescence was continued for another 40 min to obtain the maximal Mag-fluo-4 fluorescence when all of the $CaCl_2$ was released from liposomes (and DPPE-NBD fluorescence at infinite dilution). The normalized fluorescence was obtained by using the fluorescence intensity of Mag-fluo-4 (and DPPE-NBD) during fusion divided by the average intensity of Mag-fluo-4 (and DPPE-NBD) fluorescence after all of the liposomes were disrupted by n-dodecylmaltoside.

ITC Measurements. ITC experiments were performed similarly to those previously described (38). Before ITC experiments, the t-SNARE, Vn, Vc, Tomosyn C-peptide, and CDV were purified by gel filtration, using a regular or HiLoad Superdex 75 column (GE Healthcare Life Sciences) and PBS (pH 7.4) (137 mM NaCl, 3 mM KCl, 10 mM sodium phosphate dibasic, 2 mM potassium phosphate monobasic) with 0.25 mM TCEP as the running buffer, respectively. Peak fractions were pooled and concentrated. The t-SNARE and Vn, Vc, Tomosyn C-peptide, and CDV were then dialyzed in the same flask against 4 L of PBS buffer with 0.25 mM TCEP for 4 h at 4 °C and then dialyzed against another 4 L of fresh PBS buffer with 0.25 mM TCEP overnight at 4 °C. The concentrations of dialyzed proteins were determined using the Thermo Scientific Pierce Bicinchoninic Acid (BCA) protein assay kit with BSA as the standard.

ITC experiments were performed with a Microcal ITC200 instrument similarly to that described before (38). Typically, about 200 μL of t-SNARE solution was loaded into the sample cell and about 60 μL of Vn (or CDV) solution was loaded into the syringe. The heat change from each injection was integrated and then normalized by the moles of protein in the injection. The Microcal Origin ITC200 software package was used to analyze the titration calorimetric data and obtain the stoichiometric number (N), the molar binding enthalpy (ΔH), and the association constant (K_a). A nonlinear least-squares fit assuming a simple one-site chemical reaction was used. The equilibrium dissociation constant (K_D), the binding free energy (ΔG), and the binding entropy (ΔS) were calculated using the thermodynamic equations

$$K_D = \frac{1}{K_a}$$

$$\Delta G = \Delta H - T\Delta S = -RT\ln(K_a).$$

Fluorescence Anisotropy. The Vn-S28C peptide, Vc peptide, and CDV-S28C were labeled with Texas Red C2 Maleimide (Invitrogen) according the manufacturer's protocol.

Fluorescence anisotropy was measured using the PC1 photon counting spectrofluorimeter (ISS). T-format polarization was used with a 625-nm long-path filter on the left-emission channel and a monochromator on the right-emission channel. The temperature of the sample chamber was controlled with ±0.1 °C accuracy. For Texas-Red–labeled protein, the excitation wavelength was 580 nm and the emission wavelength at the right-emission channel was 612 nm. A quartz cuvette (Hellma) was used for all experiments.

To study the kinetics, ∼1 mL Texas-Red–labeled Vn-S28C solution was introduced to a quartz cuvette with continuous and rapid magnetic stirring at the desired temperature. Anisotropy was recorded as a function of time. A few microliters of cytosolic t-SNARE alone or t-SNARE prebound with Vc peptide, at various concentrations and desired temperatures, was injected into the cuvette and mixed rapidly. The data were plotted as anisotropy vs. time and the beginning of mixing was set as time 0.

To obtain the kinetics and thermodynamics parameters, we used the equations developed in a previous publication (12). For the reaction,

$$V + T \leftrightharpoons VT.$$

We have

$$\frac{dA/dt}{(A_{VT} - A_V)} = k_{on}T_0, \qquad \textbf{[S1]}$$

where k_{on} is the on rate, A is the measured anisotropy A at time t, A_V is the anisotropy of VAMP2 peptide (when all of the fluorophores are associated with VAMP2) before binding with the t-SNARE, and A_{VT} is the anisotropy of the complex (when all of the fluorophores are associated with the complex). V_0 and T_0 are the initial

concentration (or total concentration) of VAMP2 peptide and t-SNARE, respectively.

To obtain k_{on}, we performed a series of reactions such that labeled VAMP2 peptide binds to t-SNARE at various initial concentrations, T_0, and monitored the variation of A with t. For each T_0, we obtained the initial rate dA/dt from the A vs. t curve and then plotted $(dA/dt)/(A_{VT} - A_V)$ vs. T_0, which is linear, and the slope gives k_{on} (12).

When the reaction reached equilibrium, the measured anisotropy reached plateau. Let K_D be the affinity constant and A_p be the measured anisotropy at equilibrium. We have

$$A_p = A_V + (A_{VT} - A_V) \times \left\{ \frac{(K_D + V_0 + T_0) - \sqrt{(K_D + V_0 + T_0)^2 - 4V_0T_0}}{2V_0} \right\}. \quad [S2]$$

By changing the initial concentration of t-SNARE, T_0, while keeping V_0 constant, one can obtain a curve of A_p as a function of T_0. K_D is obtained using Eq. S2 and applying a nonlinear regression fit to the A_p vs. T_0 curve (12).

CD. Constructs used in the CD experiments were the minimal SNARE domains of syntaxin1A (residues 191–253), SNAP25 (SN-N residues 7–82 and SN-C residues 141–203), Vn peptide (residues 28–57), and Vc peptide (VAMP2 residues 58–94). SNARE complexes were reconstituted by incubation of equimolar ratios of individual SNAREs overnight and subsequent gel filtration chromatography (Superdex 75; GE Healthcare) with PBS and 0.2 mM TCEP. CD spectra were recorded with a Chirascan (Applied Photophysics) at 20 °C from 260 nm to 200 nm at 1-nm bandwidth.

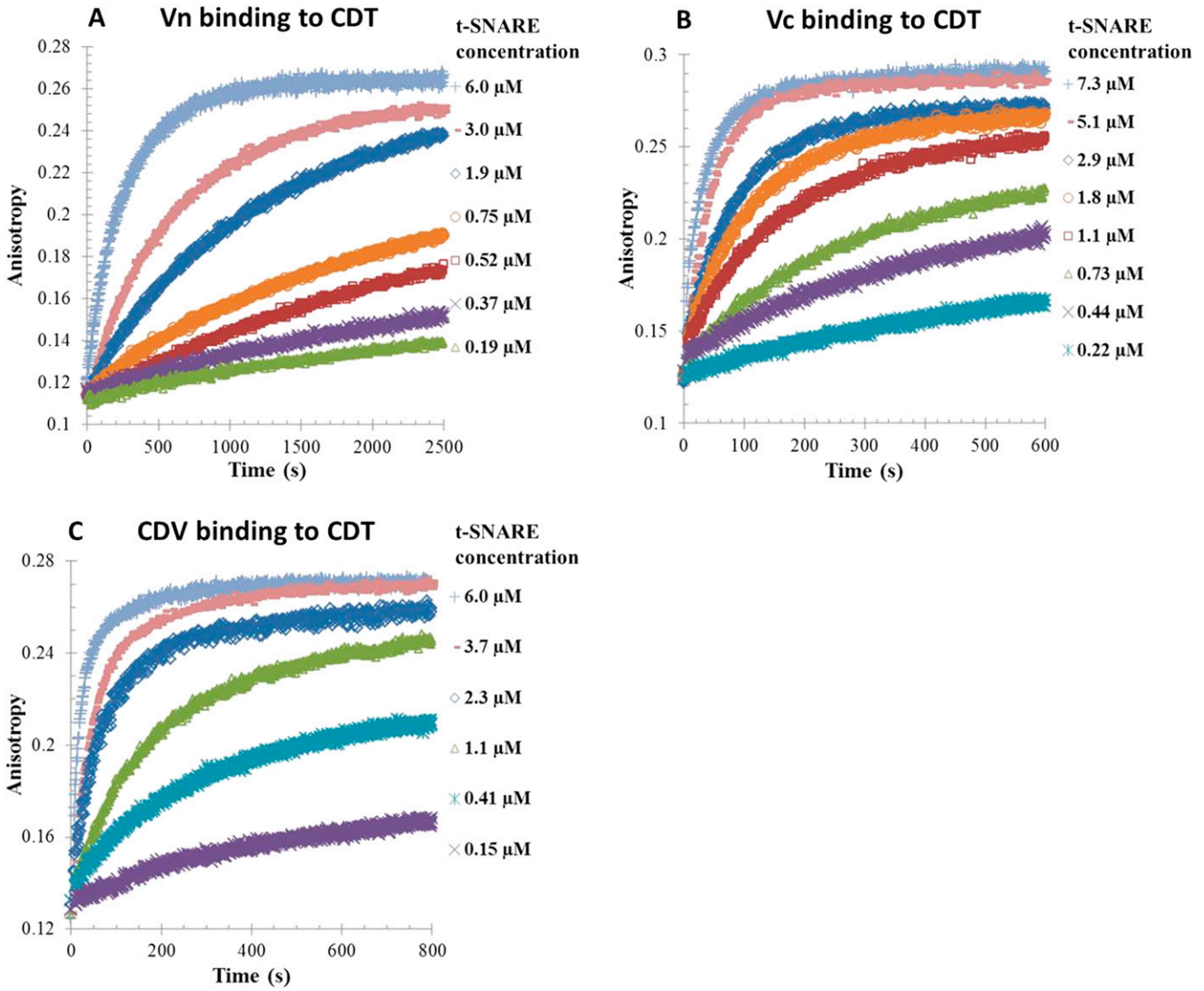

Fig. S1. Fluorescence anisotropy experiments were performed to monitor the process of a Vn peptide (*A*), a Vc peptide (*B*), or the cytosolic domain of the v-SNARE (*C*) binding to the cytosolic t-SNARE at various concentrations, respectively, at 26 °C. The Vn peptide contains VAMP2 residues 1–57 S28C and its initial concentration was 360 nM. The Vc peptide contains VAMP2 residues 58–94 and its initial concentration was 210 nM. The cytosolic domain of the v-SNARE (CDV) contains VAMP2 residues 1–94 and its initial concentration was 210 nM. All three proteins were labeled with Texas Red. An affinity constant and on rate were obtained from the curves in each panel.

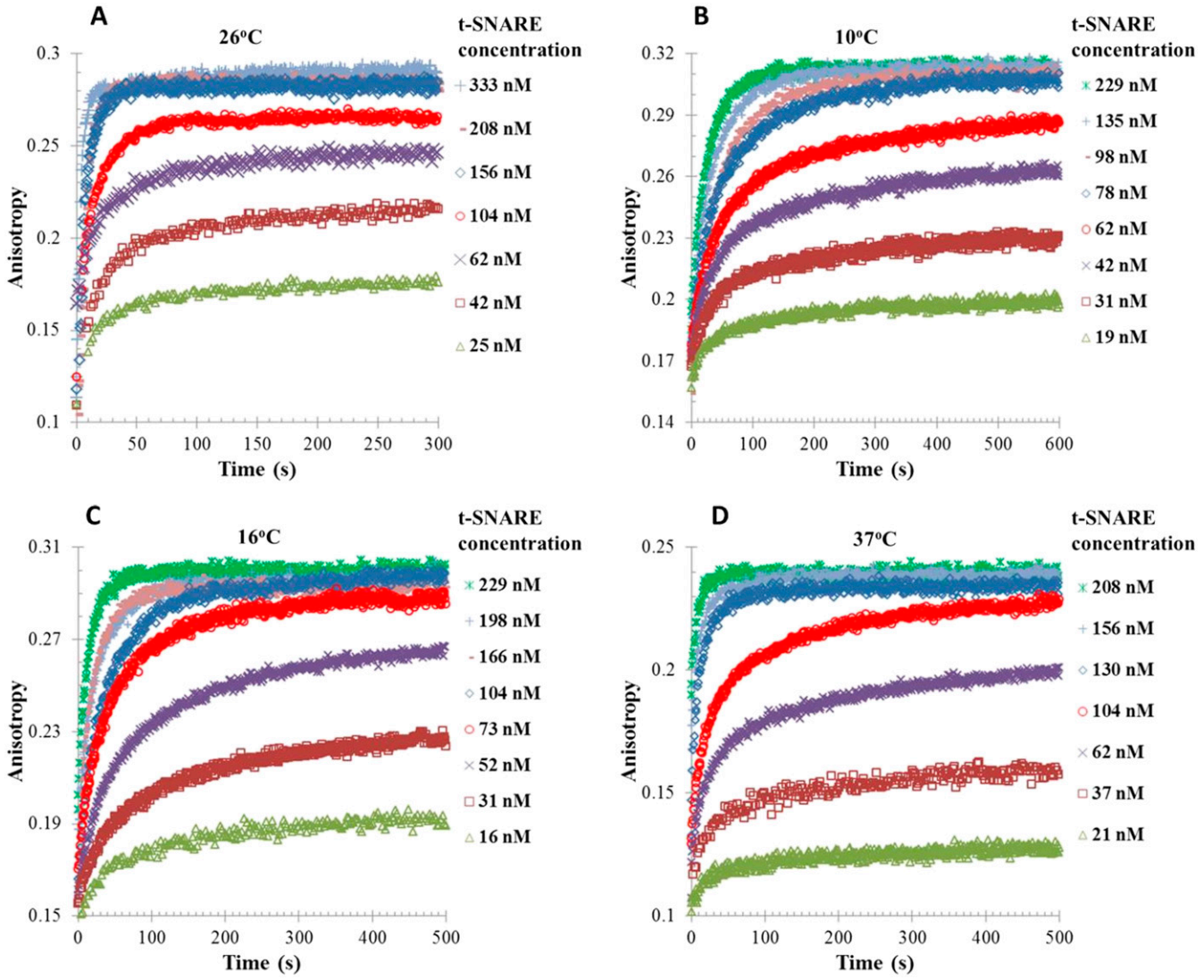

Fig. S2. Fluorescence anisotropy experiments were performed to monitor the process of a Vn peptide (VAMP2 residues 1–57 S28C) binding to the cytosolic t-SNARE prebound with a Vc peptide at various concentrations, respectively, at different temperatures: (*A*) 26 °C, where the initial concentration of Vn was 60 nM; (*B*) 10 °C, where the initial concentration of Vn was 53 nM; (*C*) 16 °C, where the initial concentration of Vn was 42 nM; and (*D*) 37 °C, where the initial concentration of Vn was 47 nM. The Vn peptide was labeled with Texas Red. The prebound t-SNARE was formed by preincubating t-SNARE and Vc peptide (molar ratio Vc:t-SNARE = 8:1) at 37 °C for 60 min. An affinity constant and on rate were obtained from the curves in each panel.

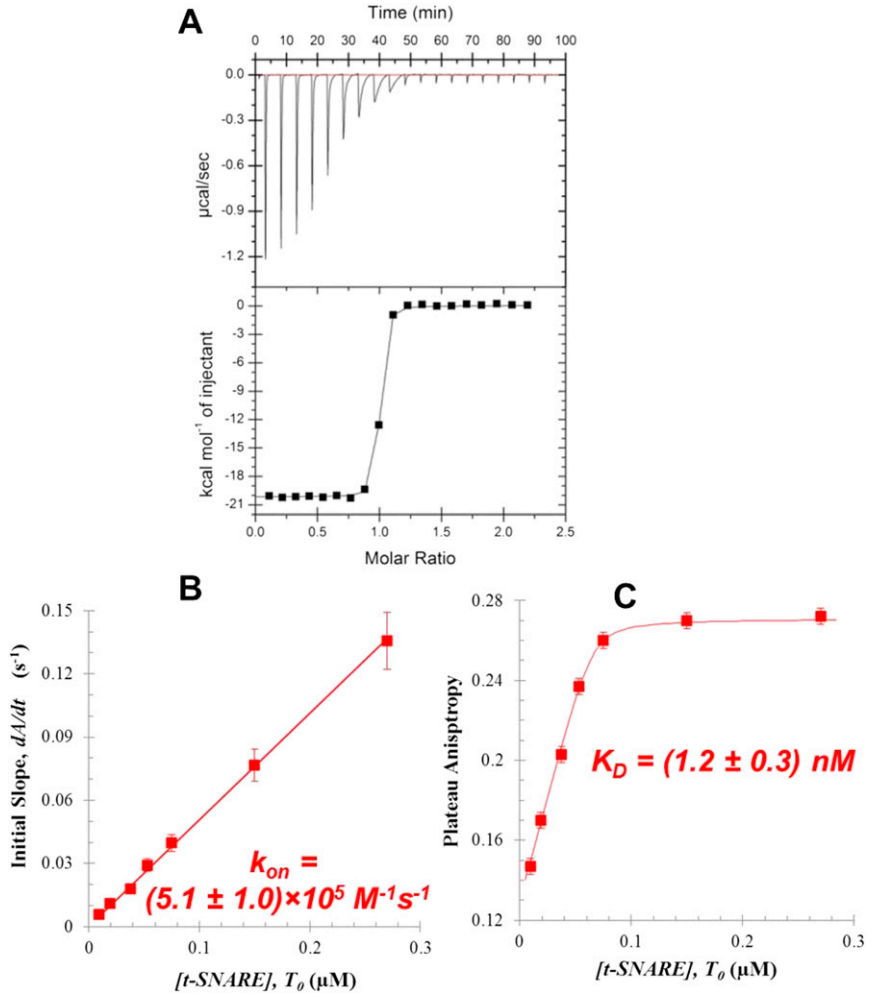

Fig. S3. Vc peptide activates the assembly between CDV and the t-SNARE. (*A*) ITC measurements of CDV assembling with prebound t-SNARE. A total of ~450 µM CDV peptide was titrated into ~42 µM prebound t-SNARE mixture. Thermodynamic parameters for the binding reaction are listed in Table S1. (*B* and *C*) Fluorescence anisotropy experiments were performed to monitor the binding process of CDV to prebound t-SNARE at various concentrations in real time. The initial binding rates were plotted vs. the concentration of t-SNARE to obtain the on rate (*B*), and the plateau anisotropy values were plotted vs. the concentration of t-SNARE to obtain the affinity constants (*C*).

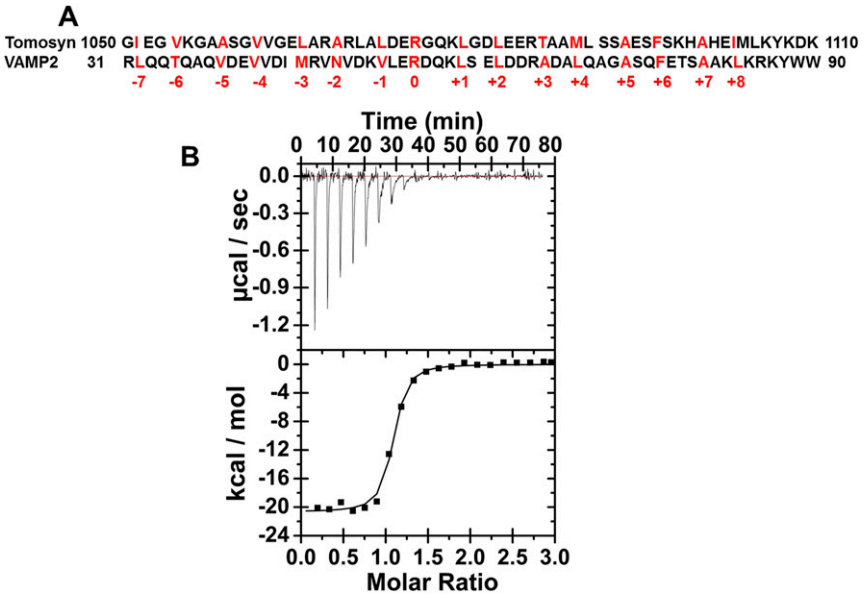

Fig. S4. Tomosyn C-peptide binds the t-SNARE. (*A*) Tomosyn contains an R-SNARE domain. Shown is comparison of the SNARE motif of Tomosyn and VAMP2. (*B*) Tomosyn C-peptide binds to the t-SNARE. In ITC measurements, ~560 μM Vn peptide was titrated into ~41 μM t-SNARE. The solid lines represented the best fit to the solid squares obtained from a nonlinear least-squares fit, assuming a simple one-site chemical reaction. Thermodynamic parameters for each binding reaction are listed in Table S1.

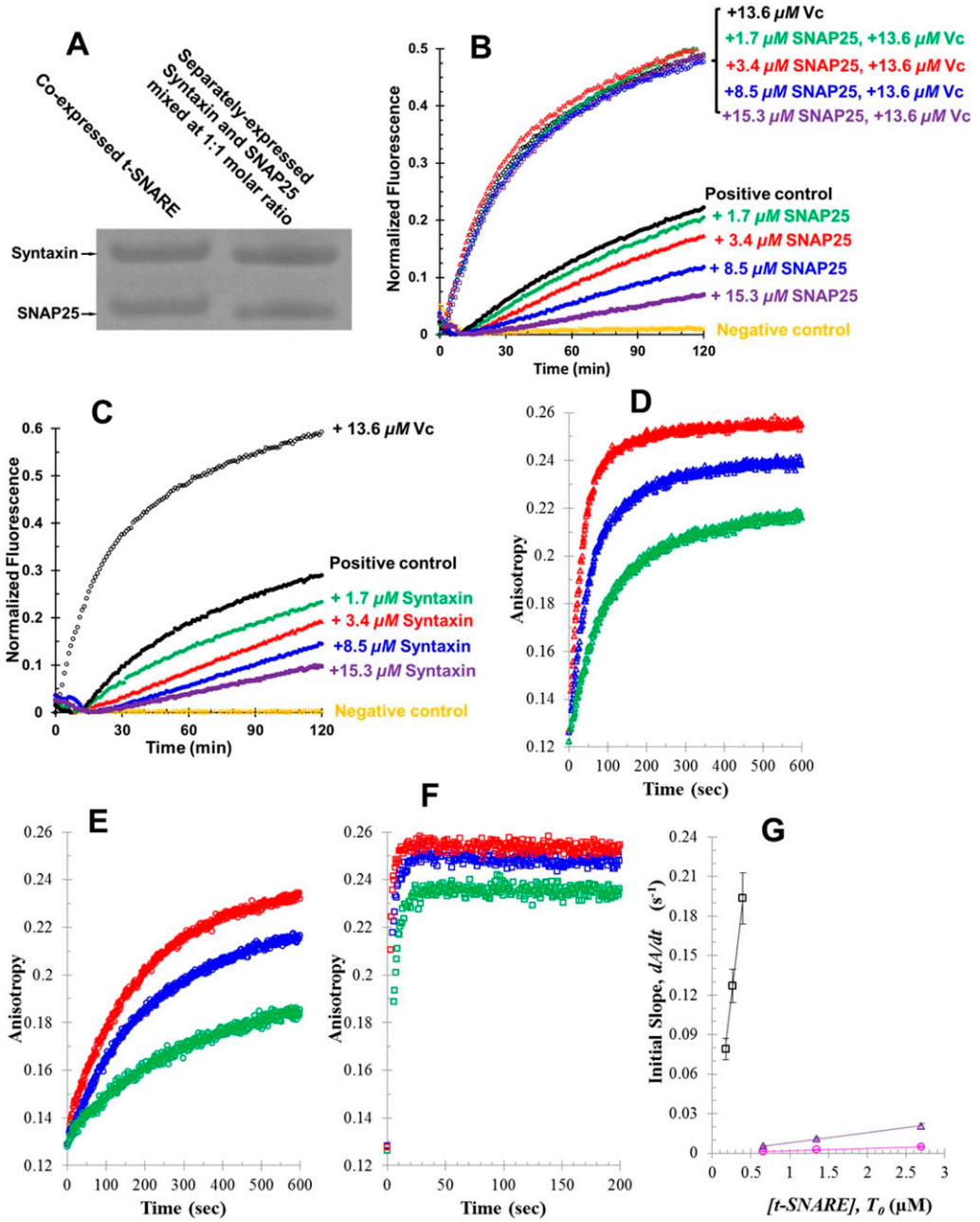

Fig. S5. Coexpressed t-SNARE contains Syntaxin and SNAP25 at 1:1 molar ratio, and assembly of SNAREs is inhibited by an excess of either Syntaxin or SNAP25. (*A*) Gel analysis of the molar ratio in coexpressed t-SNARE. Separately expressed Syntaxin and SNAP25 were mixed at a 1:1 molar ratio and loaded to the same gel together with coexpressed and copurified t-SNARE. A representative image of the gel is shown. The intensity of each protein band was quantified using ImageJ. The intensity ratio between Syntaxin and SNAP in coexpressed t-SNARE was 1.34 ± 0.05. When separately expressed Syntaxin and SNAP25 were mixed at a 1:1 molar ratio, the intensity ratio was 1.32 ± 0.04. (*B*) An excess of SNAP25 inhibits the fusion rate between t-liposomes and v-liposomes. Coexpressed full-length t-SNARE was reconstituted into liposomes and preincubated with buffer or an excess of SNAP25 at various concentrations, with or without the presence of Vc peptide at 37 °C for 30 min. After preincubation, full-length v-SNARE liposomes were added and their fusion with t-SNARE liposomes was measured. Positive control (solid black circles) represented fusion between t-liposomes and v-liposomes in the absence of extra SNAP25 or Vc. Negative control (orange crosses) showed fusion between t-liposomes preincubated with CDV and v-liposomes. (*C*) An excess of Syntaxin inhibits fusion rate between t-liposomes and v-liposomes. Coexpressed full-length t-SNARE was reconstituted into liposomes and preincubated with buffer or an excess of Syntaxin at various concentrations, with or without the presence of Vc peptide at 37 °C for 30 min. Positive control (solid black circles) showed fusion between t-liposomes and v-liposomes in the absence of extra Syntaxin or Vc. (*D*–*G*) An excess of SNAP25 slows down the assembly rate between cytosolic t-SNARE and v-SNARE. The cytosolic domain of Syntaxin (Syntaxin 1A residues 1–265) and SNAP25 were separately expressed, purified, and then mixed and preincubated for 30 min. Fluorescence anisotropy experiments were performed to monitor the process of the cytosolic domain of the v-SNARE (CDV, VAMP2 residues 1–94) binding to the mixture of Syntaxin and SNAP25 at 26 °C. CDV was labeled with Texas Red. (*D*) Syntaxin and SNAP25 were mixed at a 1:1 molar ratio at various concentrations: 2.7 μM Syntaxin and 2.7 μM SNAP25 (red triangles),1.4 μM Syntaxin and 1.4 μM SNAP25 (blue triangles), and 0.7 μM Syntaxin and 0.7 μM SNAP25 (green triangles). (*E*) Syntaxin and SNAP25 were mixed at a 1:10 molar ratio at various concentrations: 2.7 μM Syntaxin and 27 μM SNAP25 (red circles), 1.4 μM Syntaxin and 14 μM SNAP25 (blue circles), and 0.7 μM Syntaxin and 7 μM SNAP25 (green circles). (*F*) Syntaxin, SNAP25, and Vc were mixed at 1:10:8 molar ratio at various concentrations: 0.4 μM Syntaxin and 4 μM SNAP25 and 3.2 μM Vc (red squares), 0.27 μM Syntaxin and 2.7 μM SNAP25 and 2.2 μM Vc (blue squares), and 0.18 μM Syntaxin and 1.8 μM SNAP25 and 1.4 μM Vc (green squares). (*G*) The initial binding rates were plotted vs. the concentration of Syntaxin (markers). The solid lines were fits to obtain the on rates: $(7.7 \pm 1.6) \times 10^3$ $M^{-1} \cdot s^{-1}$ for Syntaxin:SNAP25 at 1:1 molar ratio (purple triangles), $(1.8 \pm 0.3) \times 10^3$ $M^{-1} \cdot s^{-1}$ for Syntaxin:SNAP25 at 1:10 molar ratio (pink circles), and $(4.8 \pm 1.0) \times 10^5$ $M^{-1} \cdot s^{-1}$ for Syntaxin:SNAP25:Vc at 1:10:8 molar ratio (black squares).

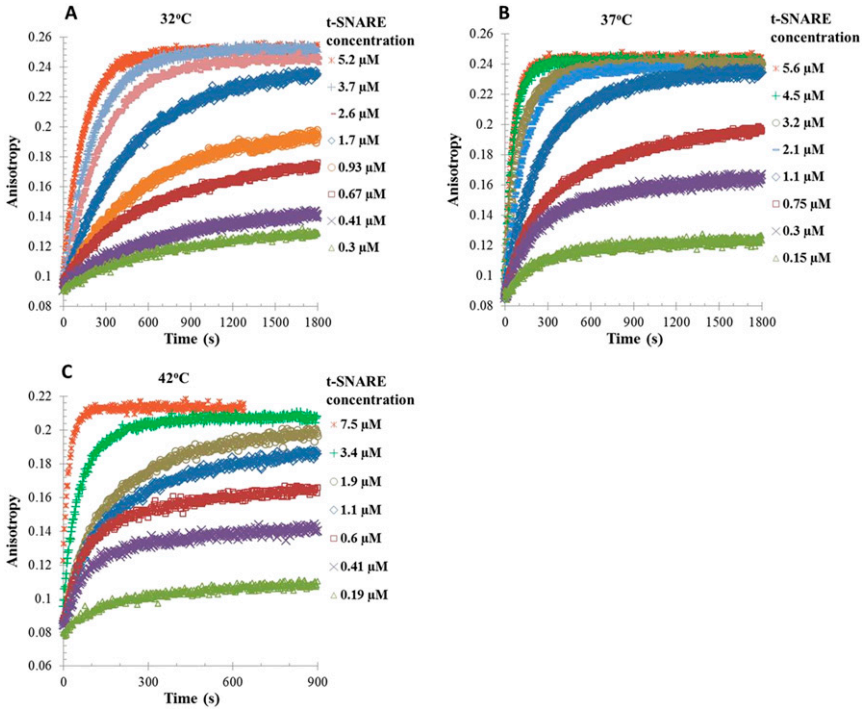

Fig. S6. Fluorescence anisotropy experiments were performed to monitor the process of a Vn peptide (VAMP2 residues 1–57 S28) binding to the cytosolic t-SNARE at various concentrations, respectively, at different temperatures: (*A*) 32 °C, where the initial concentration of Vn was 720 nM; (*B*) 37 °C, where the initial concentration of Vn was 360 nM; and (*C*) 42 °C, where the initial concentration of Vn was 170 nM. The Vn peptide was labeled with Texas Red. An affinity constant and on rate were obtained from the curves in each panel.

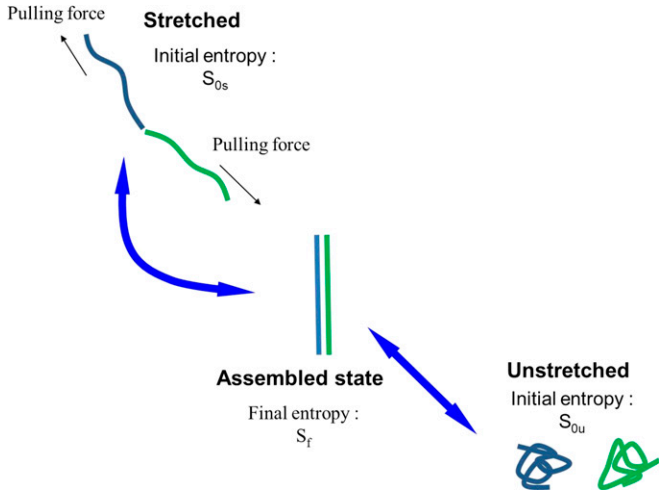

Fig. S7. In this model, both SNAREs are represented as ideal polymers. The variation of entropy from assembled to stretched is lower than the one from assembled to unstretched: $S_{0s} - S_f < S_{0u} - S_f$. Hence, it costs more free energy to form a SNARE complex when the proteins are initially unstretched (i.e., no pulling force).

Table S1. Thermodynamic parameters of protein interactions from ITC measurements

Sample cell	Titrant	N	K_D, nM	ΔH, kcal·mol^{-1}	ΔS, cal·mol^{-1}·°C^{-1}	ΔG, kcal·mol^{-1}	ΔG, k_BT
t-SNARE	Vn peptide	No observable interaction	No observable interaction	No observable interaction	No observable interaction	No observable interaction	No observable interaction
t-SNARE	Vc peptide	0.95 ± 0.01	444 ± 47	−19.1 ± 0.2	−34.9 ± 0.9	−8.7 ± 0.1	14.6 ± 0.1
t-SNARE	CDV	0.99 ± 0.01	132 ± 10	−40.1 ± 0.2	−97.8 ± 0.8	−9.8 ± 0.1	15.8 ± 0.1
t-SNARE preincubated with Vc peptide	Vn peptide	1.03 ± 0.01	6.8 ± 1.3	−20.2 ± 0.1	−30.3 ± 0.7	−11.2 ± 0.2	18.8 ± 0.2
t-SNARE preincubated with Vc peptide	CDV	0.96 ± 0.01	15 ± 3	−20.2 ± 0.1	−31.8 ± 0.8	−10.7 ± 0.1	18.0 ± 0.2
t-SNARE	Tomosyn C-terminal peptide	1.03 ± 0.01	248 ± 53	−20.7 ± 0.3	−36.4 ± 1.3	−9.4 ± 0.1	15.2 ± 0.2
t-SNARE preincubated with Tomosyn C-terminal peptide	Vn peptide	1.03 ± 0.01	14 ± 3	−20.3 ± 0.2	−29.6 ± 1.1	−11.2 ± 0.2	18.1 ± 0.2
t-SNARE preincubated with Vn peptide	Vc peptide	1.04 ± 0.01	56 ± 9	−18.9 ± 0.2	−30.0 ± 1.2	−9.9 ± 0.1	16.7 ± 0.2

Table S2. The on rates, off rates, and affinity constants of Vn and Vc peptides assembling with the t-SNARE in the absence and presence of preincubation at various temperatures, respectively, determined from fluorescence anisotropy measurements

Reaction	Temperature, °C	k_{on}, M^{-1}·s^{-1}	k_{off}, s^{-1}	K_D, nM
Vn1-57 binding to t-SNARE	26	$(5.3 \pm 1.1) \times 10^2$	$(4.5 \pm 0.9) \times 10^{-5}$	85 ± 17
	32	$(1.0 \pm 0.2) \times 10^3$	$(1.2 \pm 0.3) \times 10^{-4}$	124 ± 25
	37	$(1.9 \pm 0.4) \times 10^3$	$(2.9 \pm 0.6) \times 10^{-4}$	152 ± 30
	42	$(3.1 \pm 0.6) \times 10^3$	$(5.9 \pm 1.2) \times 10^{-4}$	187 ± 38
Vn1-57 binding to t-SNARE preincubated with Vc	10	$(3.0 \pm 0.6) \times 10^5$	$(4.8 \pm 1.0) \times 10^{-4}$	1.6 ± 0.3
	16	$(3.4 \pm 0.7) \times 10^5$	$(1.2 \pm 0.2) \times 10^{-3}$	3.5 ± 0.7
	26	$(4.9 \pm 1.0) \times 10^5$	$(2.8 \pm 0.6) \times 10^{-3}$	5.6 ± 1.1
	37	$(6.7 \pm 1.3) \times 10^5$	$(5.9 \pm 1.2) \times 10^{-3}$	8.8 ± 1.8
Vc58-94 binding to t-SNARE	26	$(6.0 \pm 1.2) \times 10^3$	$(1.0 \pm 0.2) \times 10^{-3}$	169 ± 34
	32	$(7.6 \pm 1.5) \times 10^3$	$(1.8 \pm 0.4) \times 10^{-3}$	231 ± 46
	37	$(9.3 \pm 1.9) \times 10^3$	$(3.3 \pm 0.7) \times 10^{-3}$	352 ± 70
	42	$(1.2 \pm 0.2) \times 10^4$	$(5.3 \pm 1.1) \times 10^{-3}$	444 ± 89
Vc58-94 binding to t-SNARE preincubated with Vn	10	$(3.6 \pm 0.7) \times 10^5$	$(7.0 \pm 1.4) \times 10^{-4}$	2.0 ± 0.4
	16	$(4.0 \pm 0.8) \times 10^5$	$(1.3 \pm 0.3) \times 10^{-3}$	3.3 ± 0.7
	26	$(4.7 \pm 1.0) \times 10^5$	$(3.6 \pm 0.7) \times 10^{-3}$	7.6 ± 1.5
	37	$(5.6 \pm 1.1) \times 10^5$	$(6.9 \pm 1.4) \times 10^{-3}$	12 ± 3